TOPICAL REVIEW — Physics in neuromorphic devices

Review of resistive switching mechanisms for memristive neuromorphic devices*

Rui Yang(杨蕊)†

State Key Laboratory of Material Processing and Die & Mould Technology, School of Materials Science and Engineering, Huazhong University of Science and Technology, Wuhan 430074, *China*

(Received 14 May 2020; revised manuscript received 6 July 2020; accepted manuscript online 28 July 2020)

Memristive devices have attracted intensive attention in developing hardware neuromorphic computing systems with high energy efficiency due to their simple structure, low power consumption, and rich switching dynamics resembling biological synapses and neurons in the last decades. Fruitful demonstrations have been achieved in memristive synapses neurons and neural networks in the last few years. Versatile dynamics are involved in the data processing and storage in biological neurons and synapses, which ask for carefully tuning the switching dynamics of the memristive emulators. Note that switching dynamics of the memristive devices are closely related to switching mechanisms. Herein, from the perspective of switching dynamics modulations, the mainstream switching mechanisms including redox reaction with ion migration and electronic effect have been systemically reviewed. The approaches to tune the switching dynamics in the devices with different mechanisms have been described. Finally, some other mechanisms involved in neuromorphic computing are briefly introduced.

Keywords: memristive devices, resistive switching mechanisms, neuromorphic computing

PACS: 73.61.−r, 68.37.−d, 68.55.ag **DOI:** 10.1088/1674-1056/aba9c7

1. Introduction

The development of artificial intelligence (AI) that could rival their biological counterparts, i.e., mammalian brain, has been a dream that mankind has done a lot of work to pursue. This is because the biological brain outperforms the digital computer in solving probabilistic and unstructured problems, such as cognitive and classification tasks.[1–3] As is well known, the biological neural network consists of a large number of neurons massively interconnected by an even larger number of synapses; it is the foundation of in-memory computing with massive parallelism, ultrahigh density, and low energy consumption in biological system. These years have witnessed the great progress of AI based on software neural networks with the aid of digital computers thanks to the development of algorithm.[4,5] It should be noted that the digital computer based on binary logic and serial computing has an entirely different architecture to the biological brain, costing extremely inefficient and enormous power consumption in software-based AI systems. In contrast, the hardware-based AI systems constructed by the memristive device with intrinsic dynamics resembling biological synapses and neurons are more efficient in terms of speed and power consumption. Thus, memristive devices have attracted intensive attention for neuromorphic computing in recent years.[3,6–8]

The memristive device typically has a simple sandwich structure of metal–insulator–metal (MIM), and its resistive states can be reversibly modulated according to the quantity of electric charges flowing through it.[9–11] Thus, the memristive device performs resistive switching behavior with inherent memory effect, which means its resistive state depends on not only the extra stimulations but also its intrinsic states.[12–14] Generally, the resistive switching behavior can be triggered by applying electric pules or DC voltage/current sweeping. It is found that the pinched hysteresis current–voltage (I–V) loop induced by voltage/current sweeping is the fingerprint of memristive devices.[15] Actually, a variety of resistive switching behaviors have been observed until now, and they can be classified into different types according to different criteria.[16–18] For example, the resistive switching behavior can be grouped into digital and analog categories based on the switching dynamics. Digital resistive switching describes the abrupt change between high resistive state (HRS) and low resistive state (LRS), and the abrupt current jumping appears in the I–V loop of digital cells. In contrast, the analog switching describes gradual modulation of resistive states, and continuous I–V loops are observed in the analog switching cells.[19] Note that coexistence of digital and analog switching behaviors has been reported in some devices.[20] It has been found that some devices perform analog switching behavior during voltage sweeping with low amplitude, in contrast they show

*Project supported by the National Natural Science Foundation of China (Grant Nos. U1832116 and 51772112) and Fundamental Research Funds for the Central Universities, China (Grant No. HUST: 2016YXZD058).

†Corresponding author. E-mail: yangrui@hust.edu.cn

digital switching process under voltage sweeping in high amplitude region.[21] According to the retention characteristics of the resistive states, the resistive switching behavior can be classified into volatile and nonvolatile switching groups.[22–25] As the word implies, the resistive switching occurs by electric simulations, but the switching states soon go back after removing the external simulations in volatile switching devices. In contrast, the resistive states of nonvolatile cells maintain for a long time after removing the simulations. And there also are some devices in medium states, in which the resistive state maintains for a long time but it shows partial retention loss over time, named as forgetting effect sometimes.[14,26] In addition, the resistive switching behavior can be classified into bipolar and unipolar types with respect to the electric polarity required for switching. In bipolar switching devices, the required electric pulses for SET, i.e., the change from HRS to LRS, and for RESET (the switch from LRS to HRS) have opposite polarities. Meanwhile, the SET and RESET switching shows no dependence on the polarity of the applied simulations in the unipolar switching devices.[27,28] It has been found that the resistive switching characteristics in memristive devices highly depend on the materials, device structure, external simulations, and switching mechanisms.[29–31] Thus, there are many reports about tuning the switching behavior characteristics through controlling the device structure and simulation parameters.[28,32–37]

As is well known, synapses and neurons are building blocks of neural networks. In a biological system, the synapse is the specialized junction where a neuron contacts and communicates with another neuron.[38] The contact strength, i.e., synaptic weight, varies depending on the activities of relative neurons and also its own local ion dynamics, which is termed as synaptic plasticity. And, the synaptic weight modulation is analog and possesses diverse time courses ranging from milliseconds to hours, days and even the whole lifetime.[39] Thus, analog switching behavior is generally required to mimic a synapse. Both volatile and nonvolatile resistive switching behaviors have been reported to emulate a given synaptic function with certain time courses. Unlike synapses, the neuron works to integrate inputs temporally and spatially from contacted pre-synaptic neurons, evoking a temporal boost of neuron membrane potential.[40–42] If this potential reaches the threshold, a neural pulse will be generated. In contrast, subthreshold membrane potential will soon leak out in a short time. The working process of neuron mainly presents short-term dynamics, therefore volatile switching process is usually required to emulate neuron. Thus, versatile switching dynamics are required to emulate different synaptic and neuronal functions to realize neuromorphic computing.[8,13]

Note that switching dynamics are highly related to switching mechanisms in memristive devices. Till now, different switching mechanisms have been demonstrated, including redox reaction coupled with ion migration,[30] electronic effect based on electron trapping,[43] insulator–metal transition,[44,45] phase change effect,[42,46] spin-torque effect,[47] and so on. In this review, we mainly focus on the modulation of switching dynamics in the memristive devices which have been intensely investigated for neuromorphic computing. Redox reaction and electronic effect are mainly discussed here. The redox reaction can be subdivided into two types: cation and anion migration related redox reactions. In addition, perspectives for switching dynamics modulation in memristive devices with different mechanisms are discussed.

2. Cation migration and redox reaction

The cation migration based memristive devices are generally referred to as atomic switch,[48–50] electrochemical metallization cell (ECM),[51–53] or programmable metallization cell[54–56] and have attracted intensive research interests in the past two decades. Typically, an electrochemically active electrode, such as Ag or Cu, is adopted on one side of the devices and an inert counter electrode is utilized on the other side of the devices. The resistive switching occurs mostly through creating and annihilation of a conductive metal filament resulting from the redox reaction coupled with migration of cations in the ECM cells.[57] The operation principle in conjunction with the typical I–V curve is schematically shown in Fig. 1, using Ag as the active electrode and Pt as the counter electrode for example.[51] Ag atoms are oxidized to Ag ions (Ag^+) and subsequently dissolve into the thin film electrolyte by applying a high enough positive voltage on the active Ag electrode (Fig. 1(b)). Then, Ag^+ cations drift across the thin film under the external electric field and are reduced to Ag atoms at the counter Pt electrode (Fig. 1(c)). These Ag atoms crystallize and finally form a metal conductive bridge contacting the opposite Pt electrode, which sets the device to the LRS (Fig. 1(d)). This conductive filament will be ruptured by applying a negative voltage, resetting the device to the HRS, see Fig. 1(e). The device can be reversely switched between HRS and LRS through controlling the formation/rupture of conductive filaments by applying electric field.[35,58–60]

Remarkably, dynamic growth and rupture of the conductive filaments are much more complicated in a real ECM device than the above-mentioned operation principle.[52,61] In fact, different filament growth modes, like growth from the active electrode to the counter electrode, have been observed.[58,61] Thanks to the directive observation and systemically analysis of the filament dynamic growth processes, it has been found that nanoclusters are formed in the thin film

electrolyte and they exhibit diverse dynamic behaviors governed by kinetic factors including ion mobility and redox rates, leading to different filament growth modes and filament shapes in the memristive device.[52] In addition to the filaments with a cone shape, many filaments are also observed with a dendritically branched structure. And, the rupture of the filaments occurs due to the spontaneous dissolution process driven by interfacial energy minimization between the foreigner phase of the filaments and the matrix phase of the electrolyte thin films. This spontaneous dissolution process plays a domain role in the case of thin and weak filaments,[50,56] which results in the volatile switching. This volatile characteristic is disastrous for the memory storage, but it is very useful for mimicking the synaptic short-term plasticity and the threshold-firing process of neurons.[62]

Thus, the ECM device can clearly achieve both volatile and nonvolatile switches through controlling the configuration of the filaments.[22,50,62,63] Actually, it is found that the geometry of the filaments, i.e., the density and diameter of the dendritic branches, can be utilized to control the retention characteristics of the device.[62] As shown in Fig. 2, Barbera *et al*. found that the density of the filament branches can be controlled by the compliance current level (I_C) in set process in the device of Ag/Ag_2S/Pt; the higher the applied I_C is, the greater the density of branches is obtained. And, the diameter of the filaments is supposed to be related to the number of the electric pulses. The branch grows thicker and thicker with increasing the number of applied pulses. Then, the same conductance state (i.e., $G_{max} = 0.9$ mS) can be obtained by applying different numbers of electric pulses, but the sate shows different retention characteristics, see panels 1 and 3. The states with the same branches density also show different retentions, see panels 2 and 4. These results clearly indicate that the growth and rupture of filaments can be carefully tuned by controlling the operating conditions. Note that the diameter of filaments is also found to be highly related to the level of compliance current in other devices[64,65] and fragile filaments are usually obtained under low compliance current. At the same time, much more stable filaments can be obtained under high compliance current. This phenomenon is termed as the current-retention dilemma, because it becomes very hard to decrease the operating current for memory application asking for robust filaments and very hard to increase the driving current for selector application requiring fragile filaments. Recently, Zhao *et al.* first broke the current-retention dilemma through inserting graphene with controlled defects into the Ag/SiO_2 interface in SiO_2 memristive devices.[63] It was found that the quantity and size of filaments can be well modulated by graphene defect engineering due to its excellent impermeability to cations migration. The memory device with low operation current (≈ 1 μA) was obtained by inserting graphene with concentrated defects to centralize the filament distribution. At the same time, a high driving current selector (≈ 1 mA) was realized through introducing graphene with discrete defects to decentralize the filaments distribution. This proposed strategy can be applied to other ECM cells to precisely control the geometry of the filaments to realize the expected switching behaviors.

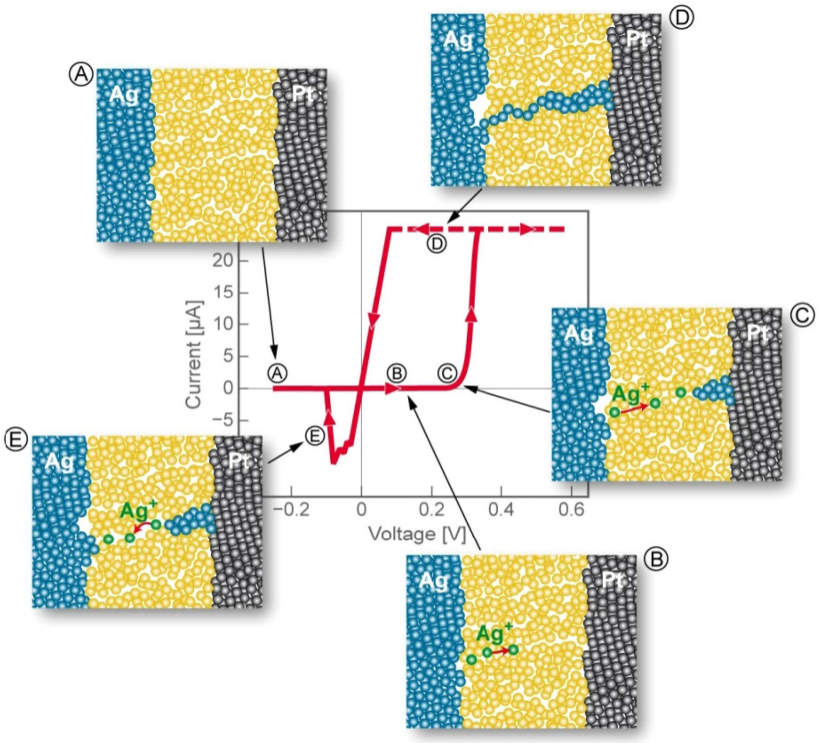

Fig. 1. Schematic operation principle of an electrochemical metallization cell in conjunction with the typical *I*–*V* curve with the SET (A–D) and RESET processes (E). Reproduced with permission.[51] Copyright 2011, IOP Publishing.

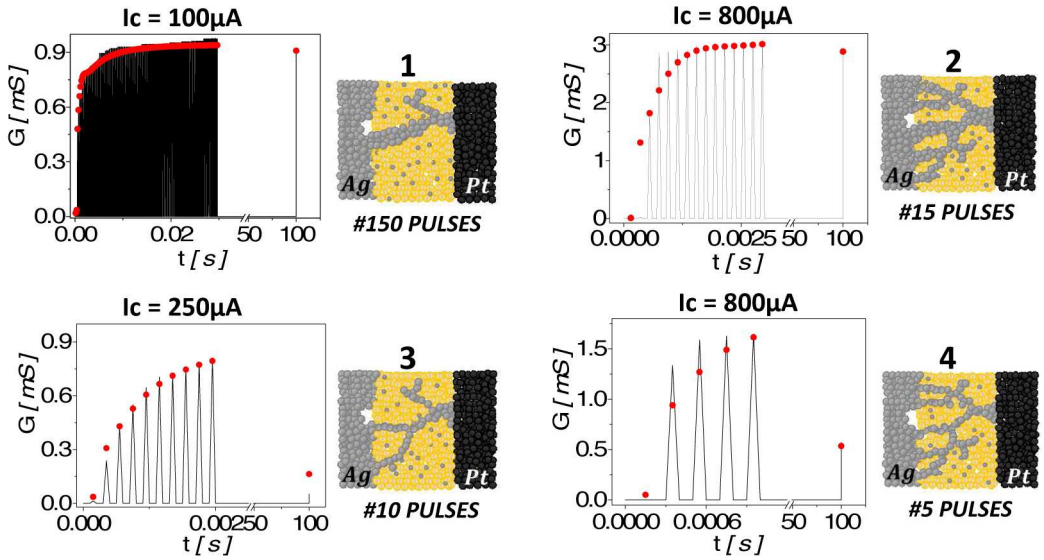

Fig. 2. The filament geometry in the device of Ag/Ag_2S/Pt, including the density and diameter of the dendritic branches, can be tuned independently through controlling the compliance current level (I_C) and number of stimulus pulses, respectively. Two implementing examples of LTP (cases 1 and 2) and STP (cases 3 and 4). Reproduced with permission.[62] Copyright 2015, American Chemical Society.

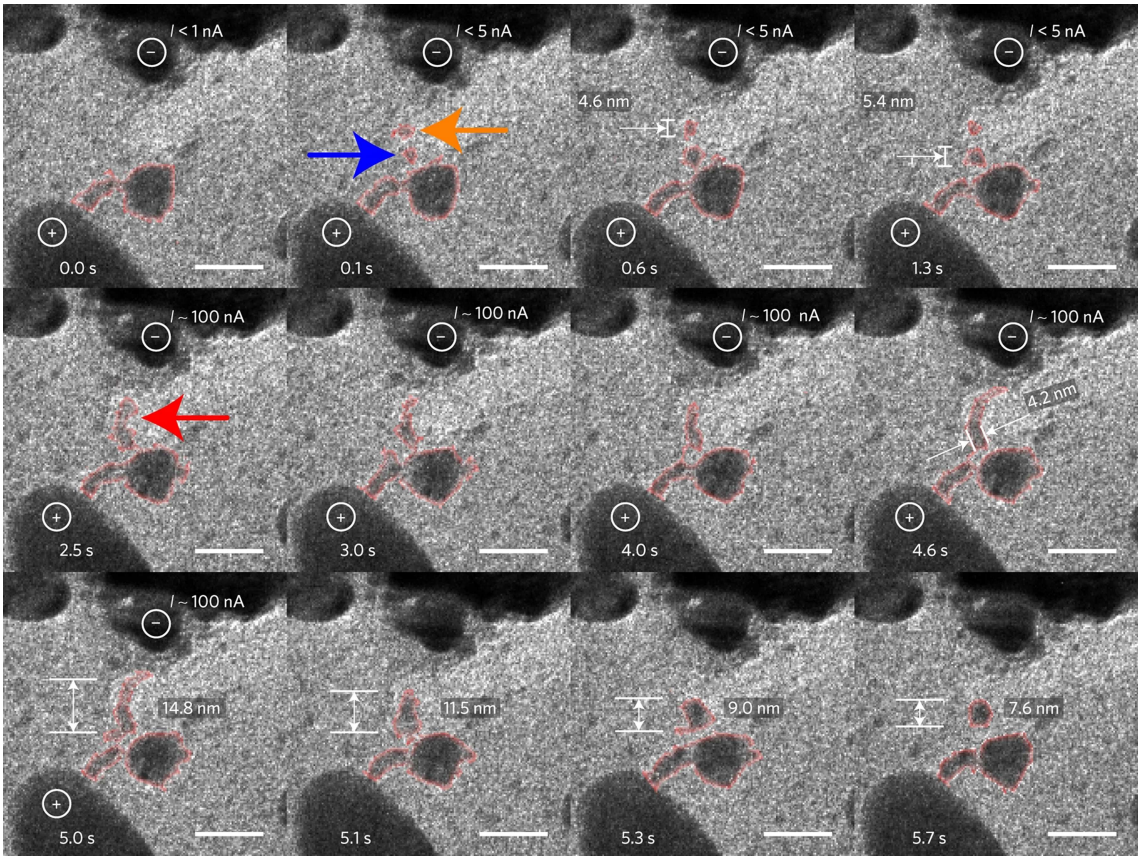

Fig. 3. *In situ* TEM observation of the planar structured Au/SiO_xN_y:Ag/Au device with threshold switching behavior, suggesting that the interfacial energy minimization induces the rapid contraction of filament after removing the external electric field. Reproduced with permission.[73] Copyright 2017, Springer Nature.

Till now, a wide range of amorphous materials have been explored as the solid electrolyte layer in the ECM cells to realize volatile and nonvolatile resistive switching behaviors, including oxides,[63,66–68] chalcogenides,[48,60,69] and organic materials.[35,70] The random uncontrollable formation and rupture of the filaments in the amorphous matrix bring the switching properties of ECM cells with unavoidable large device-to-device and cycle-to-cycle variabilities.[59] Very recently, the epitaxial single-crystalline SiGe layer was used as a switching medium to demonstrate reproducible high performance switching through confining metal filaments in a defined one-dimensional channel of threading dislocations.[31]

The volatile resistive switching behavior is also named as threshold switching. Since the typical ECM cell has an asym-

metric structure with only one active electrode in the device, the threshold switching is usually obtained when the positive voltage is applied in the active electrode.[22–25,71] Of course, some bipolar threshold switching behaviors have been observed in the typical ECM device due to the metal cations dissolved in the electrolyte working as bipolar electrodes.[27,72] Recently, the active metals were deliberately mixed in the electrolyte layer to achieve bipolar threshold switching behaviors with typical *I*–*V* curves through co-sputtering or thermal annealing technologies.[7,73] These memristive devices with bipolar threshold switching behaviors are also named as diffusive memristive devices. And, the threshold switching mechanisms have been examined through *in-situ* TEM, as shown in Fig. 3. The device is Au/SiO_xN_y:Ag/Au with a planar structure. A filament consisting of Ag nanoparticles was formed upon applying voltage from 0 s to 5 s. Then the power was turned off at 5.0 s and the conductive filament rapidly contracted under driving forces of minimizing the interfacial energy between the Ag filaments and SiO_xN_y:Ag matrix, see the pictures captured at 5.3 s and 5.7 s. These results clearly indicate that cation migration is involved in the threshold switching behavior. And these threshold switching devices find a variety of applications including selector devices for memory storage and synaptic and neuronal devices, which have gathered intensive research interest recently.[29,62,72,74]

3. Anion migration and redox reaction

Besides metal ions, anions migration, most commonly oxygen ions (typically described as oxygen vacancies, $V_{\ddot{O}}$), is involved in the memristive devices based on transition metal oxides without electrochemical active electrodes.[17,18,75–77] The migration of oxygen ions usually induces a redox reaction expressed by a valence change of the cation sublattice and leads to a stoichiometry change of the oxides. Thus, anion migration related switching mechanism is typically referred to as valence change mechanism (VCM).[10] In a VCM cell, resistive switching is generally attributed to the creation/annihilation of oxygen-deficient conductive filaments based on oxygen migration.[78,78–80] However, unlike the fruitful findings of the metal cation filaments in the ECM cells, the details of the oxygen migration and the resultant oxygen-deficient conductive filaments are still elusive and controversial owing to the difficulty in directly observing the oxygen migration process.[81–84] Thanks to intensive investigations in recent years, great progress has been made to understand the microstructure of the filaments and the dynamic oxygen migration process in switching runtime.[85]

Similar to ECM cells, an electroforming process is typically required to achieve stable resistive switching in VCM cells.[21,86] In the electroforming process, high-density oxygen vacancies are generated and migrated to form V_O-rich filaments. The atomic structure of the filaments has been confirmed to be the oxygen-deficient phase (or so-called Magnéli phase) in the TiO_{2-x}[87,88] and WO_{3-x}[89] memristive devices through TEM measurements, as shown Fig. 4. Kwon and co-authors[87] firstly observed the Ti_4O_7 filament with Magnéli phase (Fig. 4(a)) in the Pt/TiO_2/Pt devices exhibiting unipolar resistive switching behavior in 2010. In the same year, Strachan *et al.*[88] found that the Magnéli phase conductive filament was also responsible for the bipolar resistive switching process in their Pt/TiO_2/Pt devices. Unlike the filament directly bridges the top and bottom electrodes in the unipolar switching cell, the metallic Ti_4O_7 filament does not entirely span between the bottom and top electrodes due to the non-linear and low currents observed in the LRS state in their bipolar switching cell. It is proposed that there is a nano-gap and a Schottky-like barrier between the filament and the contacting electrode, as shown in Fig. 4(b). Subsequently, the resistive switching is ascribed to a modulation of the barrier due to oxygen migration under external electric field. In 2016, we also observed filaments with Magnéli phase formed in the Pt/WO_{3-x}/Pt devices in the forming process,[89] as shown in Fig. 4(c). The device had a crossbar structure and before electroforming the WO_3 thin layer was amorphous. After electroforming, a broken bubble appeared in the lower right corner of the cross point. A cross-sectional cut was made along the broken bubble and then the WO_3 thin was found crystallized and a conductive Magnéli phase was observed through TEM measurement, see panel 6 in Fig. 4(c). The subsequent bipolar resistive switching relates to the local oxygen migration in the interfacial area adjacent to the top of the filament. In 2018, Zeng *et al.* directly observed the filaments composed of monoclinic crystal with oxygen deficient in the W/HfO_x/HfO_y/Pt bilayer device. More interestingly, it was found that this monoclinic filament results from oxygen vacancy migration coupled with phase transformation of the orthorhombic phases previously formed during the forming process.[90]

In contrast, amorphous conductive filaments have been observed in many other oxide memristive devices.[83,91] Wu and co-workers[91] investigated the evolution of filaments and analyzed the filament components in the Au/Ta_2O_5/Au device through TEM and electron energy loss spectroscopy (EELS). As shown in Fig. 5(a), in the outside conducting filament region, the atomic ratio of tantalum and oxygen is nearly 2 : 5, meanwhile the ratio is nearly 1 : 2 in the filament region, which clearly demonstrates that the nano-filament is oxygen-deficient with the composition of TaO_{2-x}. The formation process of this oxygen-deficient filament is schematically illustrated in the bottom panels in Fig. 5(a) based on oxygen migration and accumulation. Recently, Kang and his coworkers[83] directly observed the nano-filament in the HfO_2-based memristive devices using TEM with electron holography, as shown in Fig. 5(b). It is found that the oxygen vacancies are generated through dissociating the Hf–O bands and the oxygen-deficient conductive filament is formed in the forming process. Subsequently, the resistive switching is achieved through the con-

nection and rupture of the filament at the top interface of the HfO_2 film.

Since oxygen vacancies are essential in the switching process in VCM cells, the asymmetric architectures using two oxide layers have been developed, in which one layer containing higher V_O concentration serves as a reservoir of V_O, while the other layer is close to stoichiometric.[92,93] A fast (10 ns) and high-endurance (10^{12} cycles) nonvolatile memristive device was demonstrated based on Ta_2O_{5-x}/TaO_{2-x} bilayer structures, see Fig. 6(a), by Samsung in 2011.[92] Through TEM and EELS measurements, they found that the superb switching performance originates from the formation and annihilation of nanoscale TaO_{1-x} filaments between a top electrode and a TaO_{2-x} base layer by means of oxygen migration, as schematically illustrated in Fig. 6(b). Meanwhile, the geometry of conductive filaments (sizes and percolation paths) in TaO_{2-x} base layer reversely changes along with the device switching process.[93]

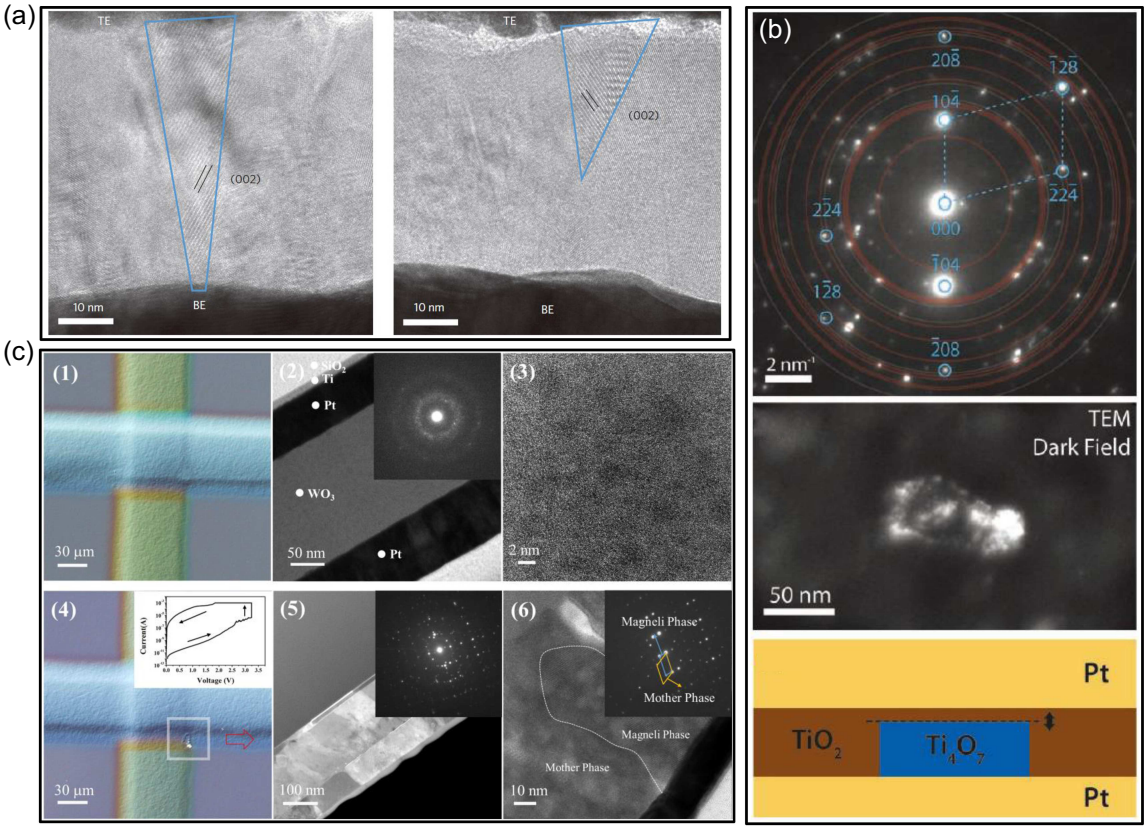

Fig. 4. Atomic structure of the conductive filaments with Magnéli structures observed in VCM cells. (a) High-resolution TEM image of a Ti_4O_7 nanofilament in the device of $Pt/TiO_2/Pt$ with unipolar resistive switching behavior. Reproduced with permission.[87] Copyright 2010, Springer Nature. (b) Electron diffraction pattern, dark field imaging of the Ti_4O_7 Magnéli crystallite and the physical model for bipolar resistive switching in the $Pt/TiO_2/Pt$ memristive devices. Reproduced with permission.[88] Copyright 2010, Wiley. (c) Structure evolution in the forming process of the $Pt/WO_3/Pt$ device, illustrating that a conductive filament with Magnéli phase is formed during the forming process. Reproduced with permission.[89] Copyright 2016, Wiley.

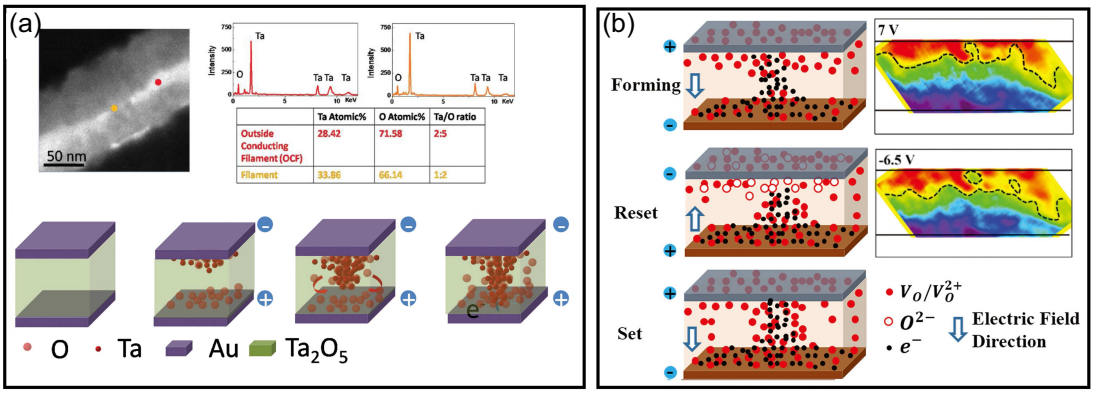

Fig. 5. Amorphous conductive filaments in VCM cells based on oxides. (a) TEM, EELS, and the physical switching mechanism for the $Au/Ta_2O_5/Au$ device. Reproduced with permission.[91] Copyright 2015, Wiley. (b) Electron holography graph of the HfO_2-based memristive device and the schematic of the switching mechanism. Reproduced with permission.[83] Copyright 2017, Wiley.

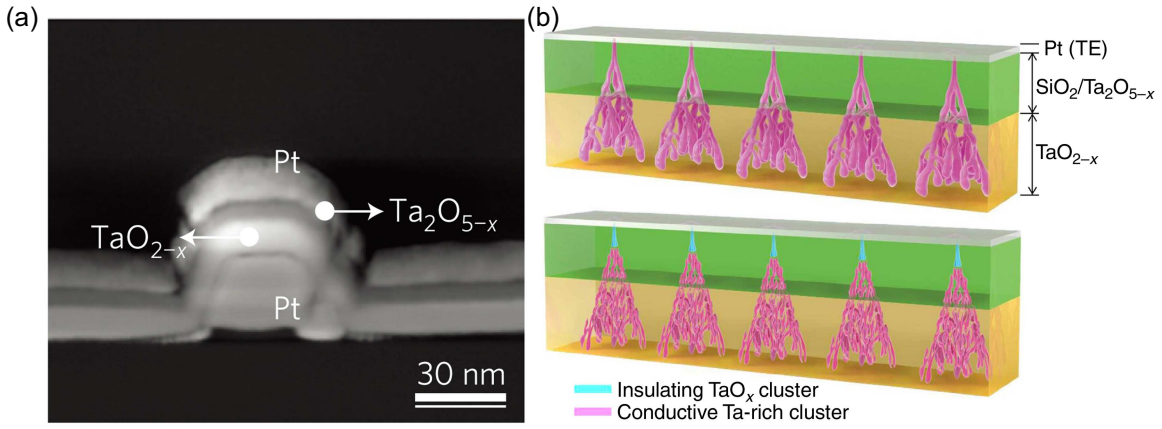

Fig. 6. Asymmetric structured memristive device with a reservoir layer of V_O and the switching mechanism of the Pt/Ta_2O_{5-x}/TaO_{2-x}/Pt device. (a) TEM image of the device. Reproduced with permission.[92] Copyright 2011, Springer Nature. (b) Schematic diagrams of formation and annihilation of nanoscale TaO_{1-x} filaments during switching. Reproduced with permission.[93] Copyright 2013, Springer Nature.

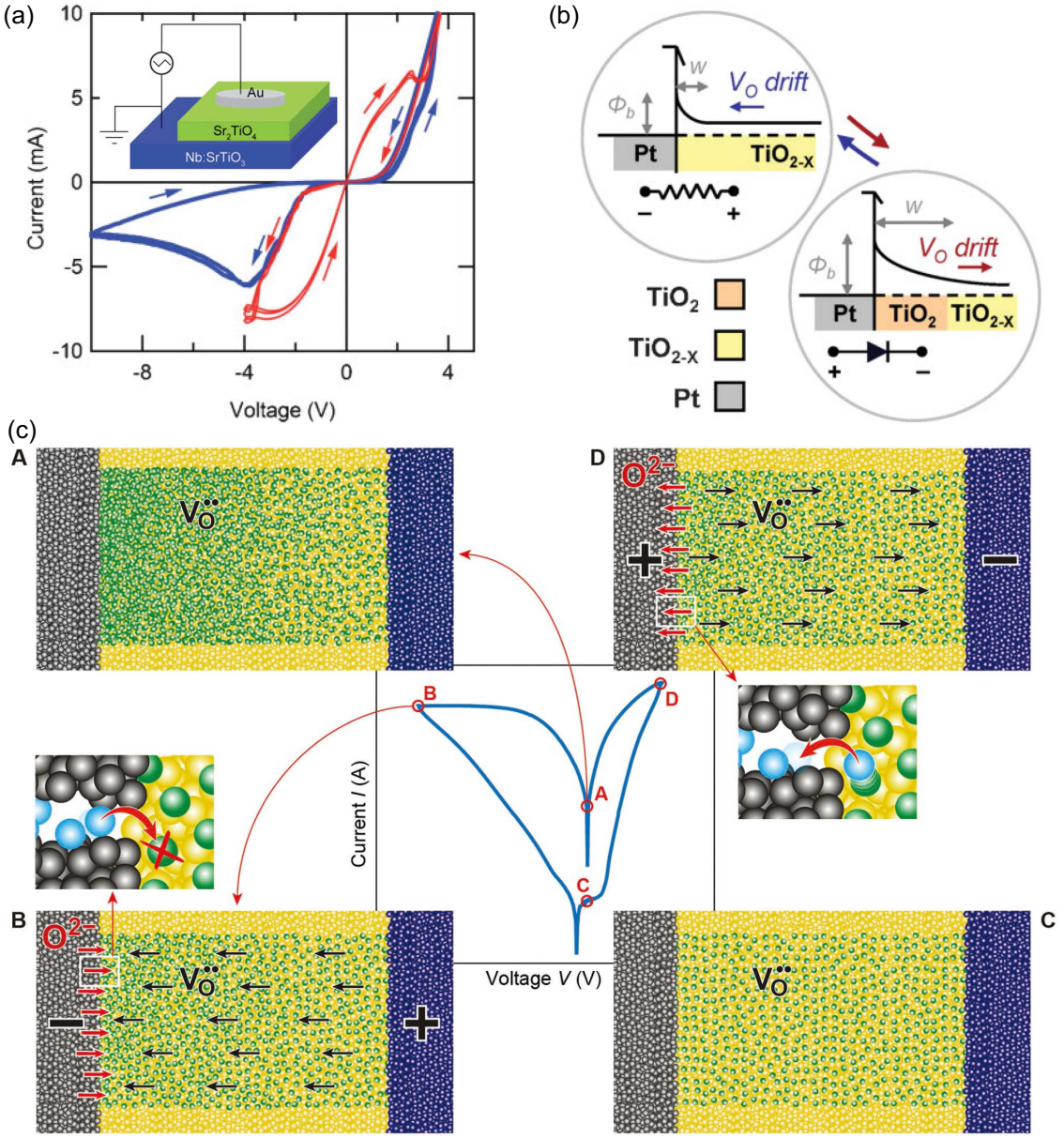

Fig. 7. Switching polarity determined by the dynamic oxygen migration process. (a) Two types of switching properties in the Au/Sr_2TiO_4/Nb:$SrTiO_3$ (STO) device; the device is schematically shown in the inset. Reproduced with permission.[32] Copyright 2010, Wiley. (b) Schematic of the switching process induced by the internal oxygen migration in the oxides. Reproduced with permission.[95] Copyright 2009, Springer Nature. (c) Schematic of switching in Pt/STO/Nb:STO device, where oxygen migrates between the top Pt electrode and the Pt/STO interface. Reproduced with permission.[102] Copyright 2017, Wiley.

In addition to the microstructure of conductive filaments in VCM cells, the dynamic oxygen migration process, including migration location and direction, has been intensively studied. Actually, the dynamic oxygen migration process determines the switching polarity in VCM cells.[32,94] For example, two types of switching properties with opposite voltage polarities were observed in one and the same device of $Au/Sr_2TiO_4/Nb:SrTiO_3$, as shown in Fig. 7(a).[32] The red curve switching shows 'counter-eightwise' polarity, whereby a device can be reset to HRS by applying positive voltage, while a negative voltage sets the device to LRS. In contrast, the blue curve switching shows 'eightwise' polarity, whereby a positive (negative) sets (resets) the device to LRS (HRS). It is worth noting that there is a Schottky-like contact at the Au/Sr_2TiO_4 interface, while an ohmic contact at the $Sr_2TiO_4/Nb:SrTiO_3$ interface. And all voltage is given on the top Pt electrode with the $Nb:SrTiO_3$ grounded, as shown in the inset in Fig. 7(a). As mentioned above, the resistive switching process in VCM cells typically is associated with local oxygen migration at the Schottky-like interface adjacent the top of switching filaments.[88] The opposite switching polarity indicates that there are two competing oxygen migration processes in one and the same device. The counter eightwise polarity switching behavior is also observed in TiO_x-based memristive devices. And, it can be explained by the internal oxygen migration within the oxides, as schematically illustrated in Fig. 7(b).[95,96] In contrast, the eightwise polarity switching cannot be explained by the internal oxygen migration within the oxides, but it is also observed in various oxides, including WO_{3-x},[97,98] CeO_2,[99] $SrTiO_3$ (STO),[100,101] HfO_x,[84] TaO_x,[81] and so on. We have proposed that the oxygen migration process mainly occurs between the Schottky-like interface and electrode in the $Pt/WO_{3-x}/Pt$ device based on the study of the atmosphere effects on the switching behavior.[97] Very recently, Cooper *et al.*[102] verified that the oxygen migrates between the top Pt electrode and the Pt/STO interface in eightwise polarity switching, as schematically shown in Fig. 7(c). In other words, oxygen is stored and electrocatalytic released in the Pt electrode during eightwise switching behavior, indicating that the oxygen migrates between the electrode and the electrode/oxides interface.

Furthermore, the actual oxygen migration microphysics is much more complicated than the drift process along the electric field.[100] It was recently found that the lateral oxygen migration in and out the conductive channels driven by radial thermophoresis and Fick diffusion, plays a key role in the eventual device switching performances, like device failure and retention characteristics, since elevated local temperature and oxygen concentration gradient are generated in the switching process.[33,103–105] And, in some typical VCM cells, it was found that the host cations are also mobile and metallic filaments can also be formed in some given VCM cells.[106,107] Therefore, it is required to consider multiple state variables involved in the switching process in a given device, though multiple variables make the switching process much more exclusive.

Actually, Lu and his coworkers[12,108] demonstrated second-order memristive devices by utilizing local temperature or oxygen ion migration mobility as a second state variable in addition to the size of filaments. Generally, these second state variables perform short-term dynamics and affect the device conductance through influencing the first state variable with long-term dynamics. The first reported second-order memristive device is $Pd/Ta_2O_{5-x}/TaO_y/Pd$,[12] in which the second state variable is the local temperature of the device. This local temperature increases abruptly due to Joule heating upon the application of a voltage pulse, then it decays spontaneously after removal of the simulation, resulting in an intrinsic internal timing mechanism. The synaptic weight modulation in biological synapses also depends on some local dynamics with short-term dynamics, such as membrane voltage and calcium time course and level. These local dynamics work as internal timing mechanisms to encode the activity information of pre- and post-synaptic neurons. Thus, the second-order memristive devices have impressive advantages over the first-order memristive devices in biorealistically mimicking synaptic plasticity. For example, the synapse emulator based on the first-order memristor asks for carefully waveform engineering and pulses overlapping to realize spike-timing dependent plasticity (STDP), because it needs to encode the relative timing information of the neuron activity to the spike amplitude or width through pulse overlapping. In contrast, biorealistical implementation of STDP can be achieved without the need of pre-/post-synaptic pulses overlapping based on the second-order memristors with intrinsic internal timing mechanisms. As a better choice for biorealistic synaptic plasticity implementation, many second-order memristors have been reported in VCM cells, including WO_x[108] and STO[13,109] based memristive devices.

Note that some VCM cells perform stable resistive switching behavior based on anion migration, but there is no filament formed in the switching process. This type of device is generally termed as interface-type, for which the resistive switching occurs at the interface over the entire electrode.[16,110,111] And, it is reported that the redox reaction occurs due to oxygen migration driven by electric field at the metal/oxides interfaces and results in reversible resistive switching. This kind of interface-type switching behavior has been reported in the $Al/Pr_{0.7}Ca_{0.3}MnO_3$ (PCMO) interface,[112] $Al/La_{0.7}Ca_{0.3}MnO_3$ (LCMO) interface,[113] and $Ti/La_{0.7}Ca_{0.3}MnO_3$ (LCMO) interface.[114] In addition, some other interface-type switching is attributed to interface barrier

modulation induced by oxygen migration in Ti/PCMO,[115] YSZ/PCMO,[116] and Pt/TiO_2.[10] Compared to fruitful results about filament-type switching cells, reports of interface-type switching are relatively limited. However, the interface-type switching device has some advantages, for example, it often requires no forming process and it is generally much more easily to achieve analog switching in the interface-type device. This is because a continuous resistive switching can be achieved by continuously modification of the device interfaces, like interfacial barrier width or height. It is worth noting that filament-type switching and interface-type switching could coexist in a given device under specific operating conditions, which offers an extra freedom to modulate the switching dynamics.[32,94]

4. Electronic effect

As aforementioned, the nanoionics-based memristive devices suffer from inevitable reliability and variability issues related to local structure distortion caused by alien or native ion migration in the switching process.[100] In contrast, electronic memristive devices, in which the resistive switching is attributed to a purely electronic process, have internal advantages in terms of switching uniformity and reliability.[43,117,118] Moreover, purely electronic memristive devices can perform switching without filaments formation/rupture, thus they have good compatibility with current mature microelectronic technology which is based on the electronic process too. Till now, electronic memristive devices have been reported in several systems mainly based on two kinds of mechanisms: charge trapping/detrapping[20,119–125] and metal–insulator transition.[34,126–130] In particular, charge traps can be subdivided into intrinsic defects, which inherently exist in the interface or the bulk of switching insulators, and extrinsic charge traps, which are artificially introduced in the switching materials including nanoparticles,[124] quantum dots,[120,123] and atom-level defects.[118] The charge trapping/detrapping process can either induce modulation of the interface barriers in the device[131,132] or changes of the bulk carrier transport process in the switching materials[121,125] and then results in the switching behavior.

Metal (with high work functions)/Nb:$SrTiO_3$ (Nb-STO) crystalline Schottky junction[122,131,133] is usually utilized as the model device to investigate the interface charge trapping induced switching behaviors, since the chemical defects have been systemically established in the Nb-STO crystalline. The analog bipolar resistive switching behavior has been experimentally demonstrated in the Au/Nb-STO,[133] Ti/Nb-STO,[122,134] and Pt/Nb-STO[131] junctions. And it is believed that the resistive switching is accompanied by a modulation of the effective height or width of the Schottky barrier through electron trapping/detrapping at the metal/Nb-STO interface. In these devices, a forward bias (i.e., the metal electrode is positively biased) sets the device from HRS to LRS and a reverse bias resets the device from LRS to HRS, as shown in Fig. 8(a).[131] In the reset process, electrons are injected from the metal electrode and trapped at the metal/Nb-STO interfaces. These negative trapped charges result in increased Schottky-barrier height and width, therefore reset the device to HRS. When the reverse bias is applied on the interface, electrons are drawn out from the traps, leaving positively charge traps in the interface. These positive charge traps provide an additional potential, which reduces the Schottky barrier height and width at the metal/Nb-STO interfaces.[133] These charge traps are proved to be interface defects induced by unintentional contaminations and metal electrode growth induced damage and/or disorder in the metal/Nb-STO interface. Mikheev *et al.*[131] experimentally demonstrated that an unintentional interface traps layer has been formed in the Pt/Nb-STO interface during Pt electrode deposition process. This interface layer can be engineered by controlling the Pt deposition method and post-annealing process.

In addition to interface barrier modulation, electron trapping/detrapping process can also induce the modulation of carrier conduction process determined by the interaction of the injected carriers and trap centers in the bulk materials, and then results in resistive switching too. Typical bulk carrier conduction processes involved in resistive switching process are the Poole–Frenkel (P–F) conduction[125] and space-charge-limited conduction (SCLC) mechanisms.[120] Take the P–F conduction process for example, the switching behavior in the Pt/Ta_2O_5/HfO_2/TiN structure observed by Yoon *et al.*[125] is explained based on the P–F conduction mechanism. In their device, the Pt/Ta_2O_5 interface has a high Schottky barrier and the HfO_2/TiN contact is quasi-Ohmic, which induce a high rectification in the *I*–*V* curves, see Fig. 8(c). It is proposed that a large number of defects have been induced in the HfO_2 layer due to the interfacial reaction with TiN layer and the damage effect during the plasma-enhanced atomic layer deposition of Ta_2O_5 on its top. As shown in Fig. 8(c), the device switches from HRS to LRS state upon positive voltage sweeping, where the voltage is applied on the top Pt electrode and bottom TiN is grounded. The device switches back from LRS to HRS by applying negative voltage sweeping. And it is found that both HRS and LRS states are mediated by P–F carrier mechanism but with different trap depths, $\sim$ 1.0 eV for HRS and $\sim$ 0.6–0.7 eV for LRS. When positive voltage is applied on the Pt electrode, the electrons are injected from the TiN electrode and trapped at the trap centers with depth of $\sim$ 1.0 eV in the HfO_2 layer. This sets the device to LRS which follows P–F conduction with trap depth $\sim$ 0.6–0.7 eV, since the deeper traps ($\sim$ 1.0 eV) are filled. When negative voltage

is applied, the Schottky barrier in the Pt/Ta_2O_5 interface efficiently suppresses the electron injection from the Pt electrode, meanwhile, the previously trapped electron in the HfO_2 layer is detrapped and drained off to the TiN electrode. Then, the device changes back to HRS which follows P–F conduction with trap depth ~ 1.0 eV. Even though there is a Schottky-barrier in this device, the resistive switching behavior results from bulk effect rather than interface barrier modulation.

The above-mentioned charge trapping/detrapping induced resistive switching behavior has been observed in many systems, including ZnO,[117] CeO_2,[135] Cu_xO,[136] ZrO_2,[137] $BiFeO_3$,[20] etc. In these devices, the energy barrier of charge detrapping determines the switching retention characteristics. The trapped electronic charge might escape from the trap sites with relatively low trapping barrier by thermally activated or tunneling process,[131] which results in an inherent retention loss, as shown in Figs. 8(b) and 8(d). At the same time, the charge-trapping site with relatively high barrier calls for high

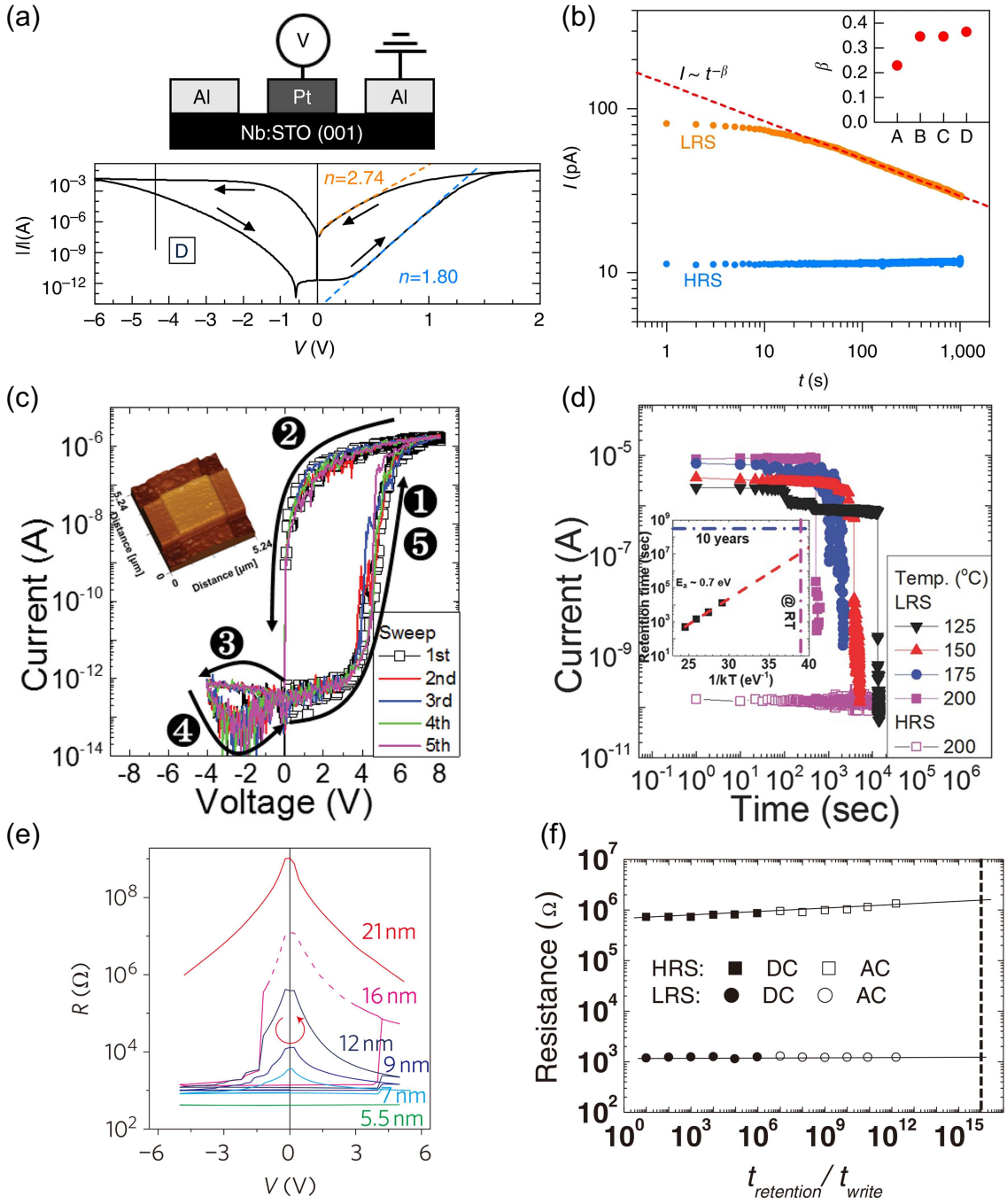

Fig. 8. Resistive switching induced by electron trapping/detrapping process. (a) *I*–*V* curve of the Pt/Nb:$SrTiO_3$/Al devics, which is set to LRS by a forward bias. Reproduced with permission.[131] Copyright 2014, Springer Nature. (b) Resistance state retention characteristics, illustrating that the electrons might escape from the trapped sites.[131] Copyright 2014, Springer Nature. (c) Resistive switching *I*–*V* curves of the Pt/Ta_2O_5/HfO_{2-x}/TiO_x/Ti sample with self-rectification. (d) Retention of the LRS and HRS at different temperatures. Reproduced with permission.[125] Copyright 2015, Wiley. (e) *I*–*V* characteristics of SiO_2:0.2Pt atomic mixtures with various thicknesses. Reproduced with permission.[118] Copyright 2011, Springer Nature. (f) Good retention performance of SiO_2:0.2Pt device at 85 °C subsequent to switching. Reproduced with permission.[43] Copyright 2011, Wiley.

energy consumption and therefore slows the switching process down. This issue is referred to as voltage–time dilemma which describes that long data retention and low-energy switching cannot be achieved simultaneously in purely electronic memristive devices.[138] This dilemma has a disastrous effect on data storage application requiring both fast switching and long retention. In contrast, this dilemma is not a terrible issue in neuromorphic computing which presents high tolerance of switching speed and data retention.

Recently, Chen and his coworkers developed a novel size-dependent metal–insulator transition nanoscale device and resolved the voltage–time dilemma faced by the normal charge-trapping electronic memristive devices.[43,118,139,140] They adopted atomic mixtures thin film of random insulators (SiO_2 or Si_3N_4) and metals (Pt, Cr, etc.) as switching medium and took the Anderson's picture of random insulators as the switching principle. As provided by Anderson, electron localization length (ζ) is finite in insulators, while it is infinite in conductors. Metal–insulator transition occurs in random mixtures with the thin films thickness (δ) comparable to ζ, across the thickness films with $\delta < \zeta$ are metallic, films with $\delta > \zeta$ are insulating, as shown in Fig. 8(e).[118] Thus, the nonvolatile and digital resistive switching is achieved through tuning ζ by charge trapping/detrapping mechanism. Specifically, the as-prepared mixture thin films are metallic. When the applied voltage reaches a threshold bias, some electrons crossing the film become trapped, erecting Coulomb repulsion as random fields and reducing ζ by ~ 10 times, which switches the device from metallic state to insulating state. The devices can switch back to the metallic state by electron detrapping through applying an opposite bias. This metal–insulator transition presents good retentions (see Fig. 8(f)), which is proposed to rely on the electron–phonon interaction to autonomously reconfigure trap-sites' barrier in accordance to the electron-occupancy of the site during the electron trapping process.[43,139]

Typically, the MIT effect results in the switching properties observed in the strongly correlated oxides (e.g., NbO_2[40,127,130] and VO_2[34,128,129]) or narrow gap Mott insulators (e.g., $GaTa_4Se_8$).[141] The basic mechanism leading to the MIT effect in a given insulator is puzzling and complicate, since it involves nontrivial out-of-equilibrium effects in the correlated systems. In the case of VO_2 and NbO_2, it is widely believed that MIT is driven by thermal effects.[142] The electric field-induced Joule heating effect can trigger a sharp resistive decrease from insulator state to metallic state when the local temperature increases across the threshold MIT temperature of the materials (e.g., 340 K for VO_2). Thus, these materials typically perform threshold switching with volatile characteristics. In other words, the metallic state will soon go back to the initial insulating state after removing the external electric field.[127] Threshold switching can also be observed in the cation migration devices based on the filaments formation/rupture, as discussed in Section 2. It is noteworthy that the turn off speed in the MIT switching device is generally much faster than that in the cation migration devices. That is because the thermal-effect-driven MIT originates from a change in lattice symmetry without ion migration. In addition to thermal effect, purely electronic mechanisms including electric-field-driven collapse of the Mott state and electronic phase separation[141] are also proposed to explain MIT effects in the correlated systems.

5. Other switching mechanisms

Even though most memristive devices can be grouped into ionic or electronic memristive devices based on their switching process driven by ion migration or electronic process. It cannot be ignored that some switching behaviors originate from the combinations of ionic migration and electronic process. Recently, Liu and his coworkers[143] demonstrated a superior MIT-driven threshold switching in a 1D VO_2 nanochannel constructed through electric-field-induced oxygen migration in the V_2O_5 thin film. It was found that ion migration in a correlated material can lead to a local MIT effect and then results in resistive switching.[76,144] In addition, the combination of ion migration and electron-trapping mechanisms is also observed in the bipolar switching behavior of the Pt/TiO_2/Pt device by Kim *et al.*[145] The formation of Ti_nO_{2n-1} filaments is attributed to oxygen migration in the forming process. After forming, the bipolar switching occurs in the local region between the top electrode and the Ti_nO_{2n-1} filament through electron trapping/detrapping process.

Note that the mechanisms discussed above mainly work in the prevalent two-terminal memristive devices. In addition to two-terminal devices, three-terminal[74,146–150] and multiple-terminal memristive devices[151] have been developed too. In the three-terminal devices, i.e., transistor-type devices, tunable and volatile channel conductivity can be obtained by controlling the gate voltage based on electrical-double layer effect[74,146,147] or electron-trapping in the channel interface.[148] The nonvolatile three-terminal device is developed using atomic switching technology.[152] In the device, the gate electrode is chemically active, while the source and drain electrodes are inert. Thus, metal cations are supplied from a gate and migrate in the channel oxides. The formation/rupture of metal filaments between the source and the drain results in nonvolatile switching behavior controlled by the gate bias. Recently, a novel battery-like three-terminal device was demonstrated to realize nonvolatile switching behaviors.[153,154] Two layers, electrolyte and channel layers, are usually inserted between gate and source. The ion inserting/extracting process occurred between the electrolyte

and channel layer induces tunable channel conductivity and therefore results in nonvolatile resistive switching process. This switching mechanism resembles charging/discharging a battery, therefore it is named as a battery-like memristive device.[155] These battery-like memristive devices possess striking switching features including low energy consumption, long retention time, and highly linear conductance response to external electric field, which provides unique opportunities for the applications of these devices in neuromorphic computing and data storage.

6. Conclusions

Given that memristive synapses and neurons require different dynamics, the underlying resistive switching mechanisms for memristive devices with different retentions, mainly ECM cells, VCM cells, and pure electronic memristive devices, are systematically discussed with typical devices and experimental results. Typically, emulation of synapses asks for analog resistive switching process. And, the switching with diverse time courses benefits the implementation of versatile synaptic plasticity. In contrast, volatile digital switching is better for emulation of neuron pulse generation process. For ECM cells, digital switching process is much easier to achieve through controlling the formation/rupture of the filaments composed of conductive cation atoms, indicating that the ECM cell naturally has advantages in neuron emulation. And, the dynamic growth and rupture of the conductive filaments, even though it varies widely in different devices, can be deliberately controlled to realize both volatile and nonvolatile switching processes. Thus, ECM cells, especially for the one with high-speed threshold switching behaviors, can be used to realize some neuron functions. It is worth noting that analog switching process can also be obtained by careful controlling the external stimulus, then some synaptic functions can also be realized based on ECM cells. Unlike ECM cells, VCM devices, especially those with interface-switching features, naturally perform analog switching behavior. Moreover, some VCM cells have more than one state variables, endowing them rich switching dynamics. Thus, VCM cells are more suitable to achieve synaptic functions especially for those synaptic functions involving both short-term and long-term dynamics. Since the VCM cell usually poses low switching speed and analog switching process, there is generally no advantages for VCM cells to emulate neuron functions compared to ECM cells. As mentioned above, the nanoionics-based memristors including both ECM cells and VCM cells suffer from unavoidable variability issues induced by ion migration. In contrast, the device based on electronic effect performs naturally uniformity. Since high uniformity of the device is required in synapses and neuron arrays for large-scale neuromorphic computing systems, memristive devices based on electronic effect possess intrinsic advantages in neuromorphic computing. Specifically, the cells based on electron trapping/detrapping generally process analog switching with diverse time courses, which are suitable for implementation of synapses. In contrast, the MIT cells with fast threshold switching behaviors benefit the realization of neuron functions.

In this review, the switching mechanisms and the approaches to adjust the switching dynamics have been discussed in detail. For ECM cells, the switching dynamics highly depend on the geometry of conductive filaments. The approaches to modulate the switching dynamics are systematically discussed, including stimulus parameters and device structure designing. For VCM cells, we mainly discuss the microstructure of conductive filaments as well as the actual oxygen migration microphysics, including migration location and directions. And multiple state variables are found to be involved in the switching process, leading to the development of the second-order memristive devices with functions better than the so-called first-order memristive device in the biorealistic implementation of the synaptic plasticity. For memristive devices based on the electronic effect, we mainly focus on the electron trapping/detrapping either at the interface or in the bulk, metal–insulator transitions in the strong correlated oxides, and the novel atomic mixtures composed of metals and random insulators. At last, other mechanisms, including the cooperation of ion migration and electronic effect, the novel switching mechanisms in three-terminal and multiple terminals are discussed.

References

[1] Strukov D B 2011 *Nature* **476** 403
[2] Versace M and Chandler B 2010 *IEEE Spectr.* **47** 30
[3] Mohammed A. Zidan Strachan J P and Lu W D 2018 *Nat. Electron.* **1** 22
[4] Merolla P A, Arthur J V, Alvarez-Icaza R, Cassidy A S, Sawada J, Akopyan F, Jackson B L, Imam N, Guo C, Nakamura Y, Brezzo B, Vo I, Esser S K, Appuswamy R, Taba B, Amir A, Flickner M D, Risk W P, Manohar R and Modha D S 2014 *Science* **345** 668
[5] Silver D, Huang A, Maddison C J, Guez A, Sifre L, van den Driessche G, Schrittwieser J, Antonoglou I, Panneershelvam V, Lanctot M, Dieleman S, Grewe D, Nham J, Kalchbrenner N, Sutskever I, Lillicrap T, Leach M, Kavukcuoglu K, Graepel T and Hassabis D 2016 *Nature* **529** 484
[6] Li C, Wang Z, Rao M, Belkin D, Song W, Jiang H, Yan P, Li Y, Lin P, Hu M, Ge N, Strachan J P, Barnell M, Wu Q, Williams R S, Yang J J and Xia Q 2019 *Nat. Mach. Intell.* **1** 49
[7] Wang Z, Joshi S, Savel'ev S, Song W, Midya R, Li Y, Rao M, Yan P, Asapu S, Zhuo Y, Jiang H, Lin P, Li C, Yoon JH, Upadhyay NK, Zhang J, Hu M, Strachan J P, Barnell M, Wu Q, Wu H, Williams R S, Xia Q and Yang J J 2018 *Nat. Electron.* **1** 137
[8] Xia Q and Yang J J 2019 *Nat. Mater.* **18** 309
[9] Strukov D B, Snider G S, Stewart D R and Williams R S 2008 *Nature* **453** 80
[10] Yang J J, Pickett M D, Li X M, Ohlberg DAA, Stewart D R and Williams R S 2008 *Nat. Nanotechnol.* **3** 429
[11] Chua L O 1971 *IEEE Trans. Circuit Theory* **18** 507
[12] Kim S, Du C, Sheridan P, Ma W, Choi S and Lu W D 2015 *Nano Lett.* **15** 2203
[13] Yang R, Huang H M, Hong Q H, Yin X B, Tan Z H, Shi T, Zhou Y X, Miao X S, Wang X P, Mi S B, Jia C L and Guo X 2018 *Adv. Funct. Mater.* **28** 1704455

[14] Xiong J, Yang R, Shaibo J, Huang H M, He HK, Zhou W and Guo X 2019 *Adv. Funct. Mater.* **29** 1807316
[15] Prodromakis T, Toumazou C and Chua L 2012 *Nat. Mater.* **11** 478
[16] Sawa A 2008 *Mater. Today* **11** 28
[17] Waser R and Aono M 2007 *Nat. Mater.* **6** 833
[18] Waser R, Dittmann R, Staikov G and Szot K 2009 *Adv. Mater.* **21** 2632
[19] Wang J and Zhuge F 2019 *Adv. Mater. Technol.* **4** 1800544
[20] Shi T, Yang R and Guo X 2016 *Solid State Ionics* **296** 114
[21] Lv F C, Yang R and Guo X 2017 *Solid State Ionics* **303** 161
[22] Chen W, Barnaby H J and Kozicki M N 2016 *IEEE Electron Device Lett.* **37** 580
[23] Du G, Li H X, Mao Q N and Ji Z G 2016 *J. Phys. D: Appl. Phys.* **49** 445105
[24] Zhao X N, Xu H Y, Wang Z Q, Zhang L, Ma J G and Liu Y C 2015 *Carbon* **91** 38
[25] Liu T, Verma M, Kang Y H and Orlowski M 2012 *Appl. Phys. Lett.* **101** 073510
[26] Kim M K and Lee J S 2018 *ACS Nano* **12** 1680
[27] Pan C B, Ji Y F, Xiao N, Hui F, Tang K C, Guo Y Z, Xie X M, Puglisi F M, Larcher L, Miranda E, Jiang L L, Shi Y Y, Valov I, McIntyre P C, Waser R, and Lanza M 2017 *Adv. Funct. Mater.* **27** 1604811
[28] Cheng C, Li Y, Zhang T, Fang Y, Zhu J, Liu K, Xu L, Cai Y, Yan X, Yang Y and Huang R 2018 *J. Appl. Phys.* **124** 152103
[29] Wang Z, Rao M, Midya R, Joshi S, Jiang H, Lin P, Song W, Asapu S, Zhuo Y, Li C, Wu H, Xia Q and Yang J J 2018 *Adv. Funct. Mater.* **28** 1704862
[30] Lee J and Lu W D 2018 *Adv. Mater.* **30** 1702770
[31] Choi S, Tan S H, Li Z F, Kim Y, Choi C, Chen P Y, Yeon H, Yu S M and Kim J 2018 *Nat. Mater.* **17** 335
[32] Shibuya K, Dittmann R, Mi S B and Waser R 2010 *Adv. Mater.* **22** 411
[33] Miao F, Yi W, Goldfarb I, Yang J J, Zhang M X, Pickett M D, Strachan J P, Medeiros-Ribeiro G and Williams R S 2012 *ACS Nano* **6** 2312
[34] Bae S H, Lee S, Koo H, Lin L, Jo B H, Park C and Wang Z L 2013 *Adv. Mater.* **25** 5098
[35] Krishnan K, Tsuruoka T, Mannequin C and Aono M 2016 *Adv. Mater.* **28** 640
[36] Li J, Duan Q, Zhang T, Yin M, Sun X, Cai Y, Li L, Yang Y and Huang R 2017 *RSC Adv.* **7** 43132
[37] Li D, Wu B, Zhu X, Wang J, Ryu B, Lu W D, Lu W and Liang X 2018 *ACS Nano* **12** 9240
[38] Pereda A E 2014 *Nat. Rev. Neurosci.* **15** 250
[39] Nicholls J G, Martin A R, Fuchs PA, Brown D A, Diamond, M E and Weisblat D A 2012 *From Neuron to Brain* (Sunderland: Sinauer Associates, Inc.) Ch. 6
[40] Pickett M D, Medeiros-Ribeiro G and Williams R S 2012 *Nat. Mater.* **12** 114
[41] Zhang X, Wang W, Liu Q, Zhao X, Wei J, Cao R, Yao Z, Zhu X, Zhang F, Lv H, Long S and Liu M 2018 *IEEE Electron Device Lett.* **39** 308
[42] Tuma T, Pantazi A, Le Gallo M, Sebastian A and Eleftheriou E 2016 *Nat. Nanotechnol.* **11** 693
[43] Choi B J, Chen ABK, Yang X and Chen I W 2011 *Adv. Mater.* **23** 3847
[44] Chudnovskii F A, Odynets L L, Pergament A L and Stefanovich G B 1996 *J. Solid State Chem.* **122** 95
[45] Torriss B, Margot J and Chaker M 2017 *Sci. Rep.* **7** 40915
[46] Karpov I, Savransky S and Karpov V 2007 *22nd IEEE Non-Volatile Semiconductor Memory Workshop*, Monterey, CA, USA, Aug.
[47] Torrejon J, Riou M, Araujo F A, Tsunegi S, Khalsa G, Querlioz D, Bortolotti P, Cros V, Yakushiji K, Fukushima A, Kubota H, Uasa S Y, Stiles M D and Grollier J 2017 *Nature* **547** 428
[48] Terabe K, Hasegawa T, Nakayama T and Aono M 2005 *Nature* **433** 47
[49] Aono M and Hasegawa T 2010 *Proc. IEEE* **98** 2228
[50] Hasegawa T, Ohno T, Terabe K, Tsuruoka T, Nakayama T, Gimzewski J K, and Aono M 2010 *Adv. Mater.* **22** 1831
[51] Valov I, Waser R, Jameson J R and Kozicki M N 2011 *Nanotechnology* **22** 254003
[52] Yang Y, Gao P, Li L, Pan X, Tappertzhofen S, Choi S, Waser R, Valov I and Lu W D 2014 *Nat. Commun.* **5** 4232
[53] Valov I and Lu W D 2016 *Nanoscale* **8** 13828
[54] Kozicki M N, Park M and Mitkova M 2005 *IEEE Trans. Nanotechnol.* **4** 331
[55] Russo U, Kamalanathan D, Ielmini D, Lacaita A L and Kozicki M N 2009 *IEEE Trans. Electron Devices* **56** 1040
[56] Hsiung C P, Liao H W, Gan J Y, Wu T B, Hwang J C, Chen F and Tsai M J 2010 *ACS Nano* **4** 5414
[57] Valov I 2014 *Chemelectrochem* **1** 26
[58] Liu Q, Sun J, Lv H B, Long S B, Yin K B, Wan N, Li Y T, Sun L T and Liu M 2012 *Adv. Mater.* **24** 1844
[59] Sun Y, Song C, Yin J, Chen X, Wan Q, Zeng F and Pan F 2017 *ACS Appl. Mater. Inter.* **9** 34064
[60] Choi SJ, Park G S, Kim K H, Cho S, Yang W Y, Li X S, Moon J H, Lee K J and Kim K 2011 *Adv. Mater.* **23** 3272
[61] Yang Y, Gao P, Gaba S, Chang T, Pan X and Lu W 2012 *Nat. Commun.* **3** 732
[62] La Barbera S, Vuillaume D and Alibart F 2015 *ACS Nano* **9** 941
[63] Zhao X, Ma J, Xiao X, Liu Q, Shao L, Chen D, Liu S, Niu J, Zhang X, Wang Y, Cao R, Wang W, Di Z, Lv H, Long S and Liu M 2018 *Adv. Mater.* **30** 1705193
[64] Sun H, Liu Q, Li C, Long S, Lv H, Bi C, Huo Z, Li L and Liu M 2014 *Adv. Funct. Mater.* **24** 5679
[65] Zhao X, Liu S, Niu J, Liao L, Liu Q, Xiao X, Lv H, Long S, Banerjee W, Li W, Si S and Liu M 2017 *Small* **13** 1603948
[66] Woo J, Lee D, Cha E, Lee S, Park S and Hwang H 2014 *IEEE Electron Device Lett.* **35** 60
[67] Tsuruoka T, Terabe K, Hasegawa T, Valov I, Rainer W and Aono M 2012 *Adv. Funct. Mater.* **22** 70
[68] Tappertzhofen S, Valov I, Tsuruoka T, Hasegawa T, Waser R and Aono M 2013 *ACS Nano* **7** 6396
[69] Xu Z, Bando Y, Wang W L, Bai X D and Golberg D 2010 *ACS Nano* **4** 2515
[70] Wu S M, Tsuruoka T, Terabe K, Hasegawa T, Hill J P, Ariga K and Aono M 2011 *Adv. Funct. Mater.* **21** 93
[71] Liu D Q, Cheng H F, Wang G, Zhu X and Wang N N 2013 *J. Appl. Phys.* **114** 154906
[72] Song J, Woo J, Prakash A, Lee D and Hwang H 2015 *IEEE Electron Device Lett.* **36** 681
[73] Wang Z, Joshi S, Savel'ev S E, Jiang H, Midya R, Lin P, Hu M, Ge N, Strachan J P, Li Z, Wu Q, Barnell M, Li G L, Xin H L, Williams R S, Xia Q and Yang J J 2017 *Nat. Mater.* **16** 101
[74] Jiang H, Belkin D, Savel'ev S E, Lin S Y, Wang Z R, Li Y N, Joshi S, Midya R, Li C, Rao M Y, Barnell M, Wu Q, Yang J J and Xia Q F 2017 *Nat. Commun.* **8** 882
[75] You T, Du N, Slesazeck S, Mikolajick T, Li G, Bürger D, Skorupa I, Stöcker H, Abendroth B, Beyer A, Volz K, Schmidt O G and Schmidt H 2014 *ACS Appl. Mater. Inter.* **6** 19758
[76] Shi J, Ha S D, Zhou Y, Schoofs F and Ramanathan S 2013 *Nat. Commun.* **4** 2676
[77] Liu H, Dong Y, Cherukara M J, Sasikumar K, Narayanan B, Cai Z, Lai B, Stan L, Hong S, Chan M K Y, Sankaranarayanan S, Zhou H and Fong D D 2018 *ACS Nano* **12** 4938
[78] Lubben M, Wiefels S, Waser R and Valov I 2018 *Adv. Electron. Mater.* **4** 1700458
[79] Yao LD, Inkinen S and van Dijken S 2017 *Nat. Commun.* **8** 14544
[80] Lenser C, Patt M, Menzel S, Kohl A, Wiemann C, Schneider C M, Waser R and Dittmann R 2014 *Adv. Funct. Mater.* **24** 4466
[81] Moors M, Adepalli K K, Lu Q Y, Wedig A, Baumer C, Skaja K, Arndt B, Tuller H L, Dittmann R, Waser R, Yildiz B and Valov I 2016 *ACS Nano* **10** 1481
[82] Mehonic A, Buckwell M, Montesi L, Munde M S, Gao D, Hudziak S, Chater R J, Fearn S, McPhail D, Bosman M, Shluger A L and Kenyon A J 2016 *Adv. Mater.* **28** 7486
[83] Li C, Gao B, Yao Y, Guan X X, Shen X, Wang Y G, Huang P, Liu L F, Liu X Y, Li J J, Gu C Z, Kang J F and Yu R C 2017 *Adv. Mater.* **29** 1602976
[84] Tian H, Chen H Y, Gao B, Yu S M, Liang J L, Yang Y, Xie D, Kang J F, Ren T L, Zhang Y G and Wong H 2013 *Nano Lett.* **13** 651
[85] Yang Y C and Huang R 2018 *Nat. Electron.* **1** 274
[86] Yang J J, Miao F, Pickett M D, Ohlberg D, Stewart D R, Lau C N and Williams R S 2009 *Nanotechnology* **21** 215201
[87] Kwon D H, Kim K M, Jang J H, Jeon J M, Lee M H, Kim G H, Li X S, Park G S, Lee B, Han S, Kim M and Hwang C S 2010 *Nat. Nanotechnol.* **5** 148
[88] Strachan J P, Pickett M D, Yang J J, Aloni S, Kilcoyne A, Medeiros-Ribeiro G and Williams R S 2010 *Adv. Mater.* **22** 3573
[89] Tan Z H, Yang R, Terabe K, Yin X B, Zhang X D and Guo X 2016 *Adv. Mater.* **28** 377

[90] Yin J, Zeng F, Wan Q, Li F, Sun Y M, Hu Y D, Liu J L, Li G Q and Pan F 2018 *Adv. Funct. Mater.* **28** 1706927
[91] Chen J Y, Huang C W, Chiu C H, Huang Y T and Wu W W 2015 *Adv. Mater.* **27** 5028
[92] Lee M J, Lee C B, Lee D, Lee S R, Chang M, Hur J H, Kim Y B, Kim C J, Seo D H, Seo S, Chung U I, Yoo I K and Kim K 2011 *Nat. Mater.* **10** 625
[93] Park G S, Kim Y B, Park S Y, Li X S, Heo S, Lee M J, Chang M, Kwon J H, Kim M, Chung U I, Dittmann R, Waser R and Kim K 2013 *Nat. Commun.* **4** 2382
[94] Muenstermann R, Menke T, Dittmann R and Waser R 2010 *Adv. Mater.* **22** 4819
[95] Yang J J, Borghetti J, Murphy D, Stewart D R and Williams R S 2009 *Adv. Mater.* **21** 3754
[96] Janousch M, Meijer G I, Staub U, Delley B, Karg S F and Andreasson B P 2007 *Adv. Mater.* **19** 2232
[97] Yang R, Terabe K, Tsuruoka T, Hasegawa T and Aono M 2012 *Appl. Phys. Lett.* **100** 231603
[98] Yang R, Terabe K, Liu G, Tsuruoka T, Hasegawa T, Gimzewski J K and Aono M 2012 *ACS Nano* **6** 9515
[99] Gao P, Wang Z Z, Fu W Y, Liao ZL, Liu K H, Wang W L, Bai X D and Wang E 2010 *Micron* **41** 301
[100] Baeumer C, Valenta R, Schmitz C, Locatelli A, Mentes T O, Rogers S P, Sala A, Raab N, Nemsak S, Shim M, Schneider C M, Menzel S, Waser R and Dittmann R 2017 *ACS Nano* **11** 6921
[101] Park J, Kwon D H, Park H, Jung C U and Kim M 2014 *Appl. Phys. Lett.* **105** 183103
[102] Cooper D, Baeumer C, Bernier N, Marchewka A, La Torre C, Dunin-Borkowski R E, Menzel S, Waser R and Dittmann R 2017 *Adv. Mater.* **29** 1700212
[103] Kumar S, Graves C E, Strachan J P, Grafals E M, Kilcoyne A L, Tyliszczak T, Weker J N, Nishi Y and Williams R S 2016 *Adv. Mater.* **28** 2772
[104] Kumar S, Wang Z W, Huang X P, Kumari N, Davila N, Strachan J P, Vine D, Kilcoyne ALD, Nishi Y and Williams R S 2016 *ACS Nano* **10** 11205
[105] Miao F, Strachan J P, Yang J J, Zhang M X, Goldfarb I, Torrezan A C, Eschbach P, Kelley R D, Medeiros-Ribeiro G and Williams R S 2011 *Adv. Mater.* **23** 5633
[106] Chen J Y, Hsin C L, Huang C W, Chiu C H, Huang Y T, Lin S J, Wu W W and Chen L J 2013 *Nano Lett.* **13** 3671
[107] Wedig A, Luebben M, Cho D Y, Moors M, Skaja K, Rana V, Hasegawa T, Adepalli K K, Yildiz B, Waser R and Valov I 2016 *Nat. Nanotechnol.* **11** 67
[108] Du C, Ma W, Chang T, Sheridan P and Lu W D 2015 *Adv. Funct. Mater.* **25** 4290
[109] Xiong J, Yang R, Shaibo J, Huang H M, He H K, Zhou W and Guo X 2019 *Adv. Funct. Mater.* **29** 1807316
[110] Bagdzevicius S, Maas K, Boudard M and Burriel M 2017 *J. Electroceram.* **39** 157
[111] Ha S D and Ramanathan S 2011 *J. Appl. Phys.* **110** 071101
[112] Lee H S, Park H H and Rozenberg M J 2015 *Nanoscale* **7** 6444
[113] Yang R, Li X M, Yu W D, Gao X D, Liu X J, Cao X, Wang Q and Chen L D 2009 *J. Phys. D-Appl. Phys.* **42** 175408
[114] Yang R, Li X M, Yu W D, Gao X D, Shang D S, Liu X J, Cao X, Wang Q and Chen L D 2009 *Appl. Phys. Lett.* **95** 072105
[115] Asanuma S, Akoh H, Yamada H and Sawa A 2009 *Phys. Rev. B* **80** 235113
[116] Arndt B, Borgatti F, Offi F, Phillips M, Parreira P, Meiners T, Menzel S, Skaja K, Panaccione G, MacLaren D A, Waser R and Dittmann R 2017 *Adv. Funct. Mater.* **27** 1702282
[117] Pan R B, Li J, Zhuge F, Zhu L Q, Liang L Y, Zhang H L, Gao J H, Cao H T, Fu B and Li K 2016 *Appl. Phys. Lett.* **108** 013504
[118] Chen ABK, Kim S G, Wang Y D, Tung W S and Chen I W 2011 *Nat. Nanotechnol.* **6** 237
[119] Wang L Y, Yang J, Zhu Y, Yi M D, Xie L H, Ju R L, Wang Z Y, Liu L T, Li T F, Zhang C X, Chen Y, Wu Y N and Huang W 2017 *Adv. Electron. Mater.* **3** 1700063
[120] Choi H Y, Wu C, Bok C H and Kim T W 2017 *NPG Asia Mater.* **9** e413
[121] Shao X L, Zhou L W, Yoon K J, Jiang H, Zhao J S, Zhang K L, Yoo S and Hwang C S 2015 *Nanoscale* **7** 11063
[122] Yin X B, Tan Z H and Guo X 2015 *Phys. Chem. Chem. Phys.* **17** 134
[123] Younis A, Chu D W, Lin X, Yi J B, Dang F and Li S A 2013 *ACS Appl. Mater. Inter.* **5** 2249
[124] Yang Y C, Pan F, Zeng F and Liu M 2009 *J. Appl. Phys.* **106** 123705
[125] Yoon J H, Kim K M, Song SJ, Seok J Y, Yoon K J, Kwon D E, Park T H, Kwon Y J, Shao X and Hwang C S 2015 *Adv. Mater.* **27** 3811
[126] Kumar S, Strachan J P and Williams R S 2017 *Nature* **548** 318
[127] Kumar S, Wang Z W, Davila N, Kumari N, Norris K J, Huang X P, Strachan J P, Vine D, Kilcoyne ALD, Nishi Y and Williams R S 2017 *Nat. Commun.* **8** 658
[128] Kim J, Ko C, Frenzel A, Ramanathan S and Hoffman J E 2010 *Appl. Phys. Lett.* **96** 213106
[129] Lee S B, Kim K, Oh J S, Kahng B and Lee J S 2013 *Appl. Phys. Lett.* **102** 063501
[130] Park J, Yoo J, Song J, Sung C and Hwang H 2018 *IEEE Electron Device Lett.* **39** 1171
[131] Mikheev E, Hoskins B D, Strukov D B and Stemmer S 2014 *Nat. Commun.* **5** 3990
[132] Wang J R, Pan R B, Cao H T, Wang Y, Liang L Y, Zhang H L, Gao J H and Zhuge F 2016 *Appl. Phys. Lett.* **109** 143505
[133] Yan ZB and Liu J M 2013 *Sci. Rep.* **3** 2482
[134] Goossens A S, Das A and Banerjee T 2018 *J. Appl. Phys.* **124** 152102
[135] Kim H J, Zheng H, Park J S, Kim D H, Kang C J, Jang J T, Kim D H and Yoon T S 2017 *Nanotechnology* **28** 285203
[136] Fang T N, Kaza S, Haddad S, Chen A, Wu Y C, Lan Z, Avanzino S, Liao D, Gopalan C and Choi S 2006 *Electron Devices Meeting* San Francisco, CA, USA, Dec., 2006
[137] Liu Q, Guan W, Long S, Jia R, Liu M and Chen J 2008 *Appl. Phys. Lett.* **92** 012117
[138] Schroeder H, Zhirnov V V, Cavin R K and Waser R 2010 *J. Appl. Phys.* **107** 054517
[139] Yang X, Tudosa J, Choi B J, Chen A and Chen I W 2014 *Nano Lett.* **14** 5058
[140] Yang X, Choi B J, Chen A and Chen I W 2013 *ACS Nano* **7** 2302
[141] Dubost V, Cren T, Vaju C, Cario L, Corraze B, Janod E, Debontridder F, and Roditchev D 2013 *Nano Lett.* **13** 3648
[142] Kim H T, Chae B G, Youn D H, Maeng S L, Kim G, Kang K Y and Lim Y S 2004 *New J. Phys.* **6** 52
[143] Xue W, Liu G, Zhong Z, Dai Y, Shang J, Liu Y, Yang H, Yi X, Tan H and Pan L 2017 *Adv. Mater.* **29** 1702162
[144] Rozenberg M J, Inoue I H and Sanchez M J 2004 *Phys. Rev. Lett.* **92** 178302
[145] Kim K M, Choi B J, Lee M H, Kim G H, Song S J, Seok J Y, Yoon J H, Han S and Hwang C S 2011 *Nanotechnology* **22** 254010
[146] Zhu L Q, Wan C J, Guo L Q, Shi Y and Wan Q 2014 *Nat. Commun.* **5** 3158
[147] Zang Y, Shen H, Huang D, Di C A and Zhu D 2017 *Adv. Mater.* **29** 1606088
[148] Tian H, Mi W, Wang X F, Zhao H, Xie Q Y, Li C, Li Y X, Yang Y and Ren T L 2015 *Nano Lett.* **15** 8013
[149] Liu C, Yan X, Song X, Ding S, Zhang D W and Zhou P 2018 *Nat. Nanotechnol.* **13** 404
[150] Liu CS, Chen H W, Hou X, Zhang H, Han J, Jiang Y G, Zeng X Y, Zhang D W and Zhou P 2019 *Nat. Nanotechnol.* **14** 662
[151] Wan C J, Feng P, Wang W, Zhu L Q, Liu Z P, Shi Y and Wan Q 2016 *Adv. Mater.* **28** 5878
[152] Wang Q, Itoh Y, Tsuruoka T, Aono M and Hasegawa T 2015 *Adv. Mater.* **27** 6029
[153] van de Burgt Y, Lubberman E, Fuller E J, Keene S T, Faria G C, Agarwal S, Marinella M J, Talin A A and Salleo A 2017 *Nat. Mater.* **16** 414
[154] Fuller E J, El Gabaly F, Leonard F, Agarwal S, Plimpton S J, Jacobs-Gedrim R B, James C D, Marinella M J and Talin A A 2017 *Adv. Mater.* **29** 1604310
[155] Yang J J and Xia Q 2017 *Nat. Mater.* **16** 396